ADVANCED ELECTRONIC MATERIALS
www.advelectronicmat.de

Submicron Vertical Channel Organic Electrochemical Transistors with Ultrahigh Transconductance

Dimitrios A. Koutsouras, Fabrizio Torricelli, and Paul W.M. Blom**

Organic electrochemical transistors (OECTs) belong to the class of electrolyte gated organic transistors (EGOTs) that offer a smooth interface with biology in combination with high transconductance values of typically a few mS. Fabrication-wise, though, most of the up-to-date reported devices are limited to two dimensional structures, where the transistor channel is patterned on the same plane as the source and drain electrodes. Here, a method is introduced for the fabrication of integrated vertical channel OECTs (vOECTs) with submicron channel length. By employing electrodeposition, a vertical channel sandwiched between the source and drain electrodes is created. Channel lengths down to 60 nm are demonstrated, giving rise to ultrahigh transconductance of up to 275 mS. Accounting for the voltage loss on the device connection tracks, an intrinsic transconductance of vOECTs of 500 mS is found. The vOECTs are three-dimensional transistors finding relevant application in "organ-on-a-chip" and implantable devices, where high amplification and small footprint are demanded.

1. Introduction

Organic materials have recently gained the increasing attention of the scientific community due to their unique set of features and the state-of-the-art devices they offer. Especially in the field of bioelectronics, conducting polymers have emerged as a strong candidate for the realization of novel devices with an improved interface with the biological world.[1–3] For example, conducting polymers have been used as coatings of electrodes for neural recording applications, both in vitro and in vivo,[4,5] for the study of metabolic diseases,[6] for cell stimulation applications,[7] and for the realization of high-performing biosensing platforms.[8]

In the last decade, attention shifted from organic coatings to organic-biology interfaces.[9] Electrolyte-gated organic transistors (EGOTs) have been used to address biological-driven paradigms, opening new routes of applications.[10] Especially, organic electrochemical transistors (OECTs) constitute a class of EGOTs where voltage changes at the interface between the electrolyte and the conducting polymer film are used to drive ions in and out of the channel and to modulate its conductivity.[11] The OECT device architecture has been exploited in a plethora of biological-related applications.[2] In particular, OECTs have been extensively used to record neuronal activity,[12,13] to offer high-performing biosensors,[14] to produce ion-selective devices,[15] and to realize neuromorphic archetypes.[16] One important characteristic of the OECT is the low operation voltage (below 1 V) and its stability in aqueous milieus.[2,3,17] Another essential feature is the ability to support miniaturized geometries that result in high integration densities, a fact that is a comparative advantage when it comes to the fabrication of high-performing bioelectronic chips. So far, most of the reported OECTs are in-plane devices, with the channel length ranging from a few microns to a few millimeters. Focusing on the integration features, a vertical channel OECT topology would be beneficial since the small device footprint enables a larger number of transistors monolithically integrated in the same substrate. These transistors, endowed with short channel lengths, would be capable to support large currents and to deliver high transconductance, eventually resulting in a large in-situ detection and amplification of the biological signals. However, exploiting the third dimension is very challenging with regard to device fabrication.

Although vertical devices have been already presented for the class of organic field effect transistors (OFETs),[18] there are very few examples of vertical OECTs. More in detail, a vertical geometry was recently proposed, in which the OECTs were realized in a step-edge transistor topology.[19,20] A vertical displacement of the source and drain electrodes, through the parylene C insulating layer of the device, acted as a spacer and defined the transistor channel. However, this approach limits the minimum attainable channel length to the thickness of the parylene C layer, typically a micron, in order not to jeopardize the device proper encapsulation. In a slightly different geometry, a vertical channel electrolyte-gated organic transistor was presented, still with an insulating silicon dioxide (SiO_2) spacer

D. A. Koutsouras, P. W.M. Blom
Department of Molecular Electronics
Max Planck Institute for Polymer Research
Ackermannweg 10, 55128 Mainz, Germany
E-mail: koutsouras@mpip-mainz.mpg.de; blom@mpip-mainz.mpg.de
F. Torricelli
Department of Information Engineering
University of Brescia
Via Branze 38, Brescia 25123, Italy

The ORCID identification number(s) for the author(s) of this article can be found under https://doi.org/10.1002/aelm.202200868.

DOI: 10.1002/aelm.202200868

separating the top and bottom electrodes, and with a diketopyrrolopyrrole–terthiophene donor–acceptor polymer (PDPP) film forming the channel.[21] Other inorganic/organic hybrid vertical channel structures were also proposed,[22] lacking, though, the advantages of a truly microfabricated device.

In this paper, we present a vertical channel organic electrochemical transistor (vOECT). With the use of microfabrication techniques, the transistor channel is sandwiched between a bottom and a top electrode that are deposited on perpendicularly overlapping planes. The conducting polymer channel, made of poly(3,4-ethylenedioxythiophene) polystyrene sulfonate (PEDOT:PSS), is formed via electrodeposition, from 3,4-ethylenedioxythiophene (EDOT) and polystyrene sulfonate (PSS). The electrodeposition enables to accurately control the polymer thickness, viz. the OECT channel length. This fabrication approach allowed us to fabricate vOECTs with channel length (L) down to the sub-100 nm scale, resulting in extremely high transconductance values. The transistor transconductance is defined as $g_\mathrm{m} = \frac{\Delta I_\mathrm{ds}}{\Delta V_\mathrm{gs}}$ and is a very important OECT figure of merit, since it is a measure of the device signal amplification.[23] Therefore, especially for biological relevant measurements, the increased transconductance results in devices with enhanced ability to record subtle biological signals. The transconductance value of 275 mS (498 mS if corrected for the voltage loss on the connection tracks) presented here, is the highest one reported up to date. The device operation principle takes advantage of the electrolyte gating to exhibit a low-voltage operation, while the fabrication process remains compatible with organic materials fabrication protocols, a feature desirable in organic bioelectronic applications such as "organ-on-a-chip" platforms and implantable devices. In practice, it also means that a greater number of vOECTs can be integrated in the same substrate area compared with their planar counterparts, combined with an enhanced transistor performance. Finally, the electrode stacking on different perpendicular levels, one on top of the other, opens new pathways for the realization of OECT cross bar geometries with multiple applications in the development of high-density neural networks and the realization of neuromorphic paradigms.[24]

2. Results and Discussion

The vertical channel OECTs were fabricated with a combination of standard microfabrication techniques. The detailed fabrication process is presented in the Experimental Section. Briefly, optical microscope glass slides (26 mm × 76 mm) were thoroughly cleaned in soap and acetone/isopropanol baths. Photolithography was employed to define the bottom gold electrode leads on the substrate. Next, the negative photoresist SU-8 was used to insulate electrically the devices. A second photolithography step defined the active area of the bottom electrode after a ultraviolet (UV) light exposure and a selective removal of the photoresist through development. This is a very important fabrication step as it outlines the OECT channel width (W) and thickness (d). Electrodeposition was employed to coat the bottom electrode active area with PEDOT:PSS, creating the channel of the transistor. **Figure 1** presents the device geometry. Micrographs of the devices are presented in the Figure S1 (Supporting Information). Using this novel fabrication approach, the conducting polymer film thickness sets the transistor length (L). Finally, the top electrode was deposited via sputtering and patterned with a shadow mask. An intentional, slight misalignment of the top electrode lead, with respect to the bottom one, assists the electrolyte's ions to access the conducting polymer film and to de-dope it during gating.

Figure 1a shows the sideview of the OECT gated by an Ag/AgCl electrode in a liquid electrolyte (NaCl 0.1 м). The gold bottom electrode serves as the transistor source, while the top gold electrode is the drain. In between, the PEDOT:PSS channel connects the two, realizing a truly 3D geometry. It worth noticing that contrary to a typical OECT, in this configuration the conducting polymer film thickness is not the one that defines the channel thickness but rather its length, as depicted in Figure 1b. This allows for the miniaturization of the device channel to the submicron scale. Furthermore, the channel width (W) and thickness (d) are now controlled by the bottom electrode area (device top view, Figure 1c,d). This means that the product $W \times d$ can be accurately set through the microfabrication process. In addition, the channel thickness (d) can be easily set to very high values, namely 200, 500, or even 1000 µm, which, with the conventional OECT fabrication techniques, is very difficult or even impossible to be achieved. Most importantly, since the OECT transconductance g_m is proportional to the factor Wd/L, the very small L, in combination with the very high $W \times d$, can result in extremely high, previously unattainable, transconductances. Figure 1e presents a 3D projection of the vOECT revealing the vertical geometry of the channel. The whole fabrication process is depicted in Figure 1f.

Figure 2 displays typical output curves, transfer curves, and the corresponding transconductance of vertical channel OECTs with various dimensions. The steady state gate currents are presented in Figure S6 (Supporting Information).

Figure 2a shows a device with a 50 µm × 50 µm ($W \times d$) footprint and a channel length of $L = 246$ nm. For the output curves, the drain voltage sweeps from 0 to −0.6 V and the gate voltage from −0.6 V to +1 V. The transfer curve displayed in Figure 2b is typical of depletion mode OECTs. The on-current is larger than 20 mA and it is modulated by the gate voltage. Most importantly, the maximum transconductance amounts to 34 mS, which is more than one order of magnitude larger than that of conventional in-plane OECTs with the same footprint.

As expected, an increase of the device $W \times d$ factor results in an increase of the device current and its transconductance. This is demonstrated in Figure 2c,d. The OECT has a $W \times d =$ 100 µm × 100 µm and a channel length L = 210 nm. The transconductance reaches the value of 65 mS. If the patterned bottom electrode becomes as large as 200 µm × 200 µm ($W \times d$), the transistor presents a transconductance of up to 97 mS (Figure 2e,f). This means that the versatility of choosing $W \times d$ products through fabrication, and the submicron channel controlled via the films thickness, allow to easily obtain vOECTs with very high transconductance. The output characteristics also show the lack of drain-current saturation. The transistors remain in the ohmic region for every applied gate voltage. This is due to the very small channel length and has been reported

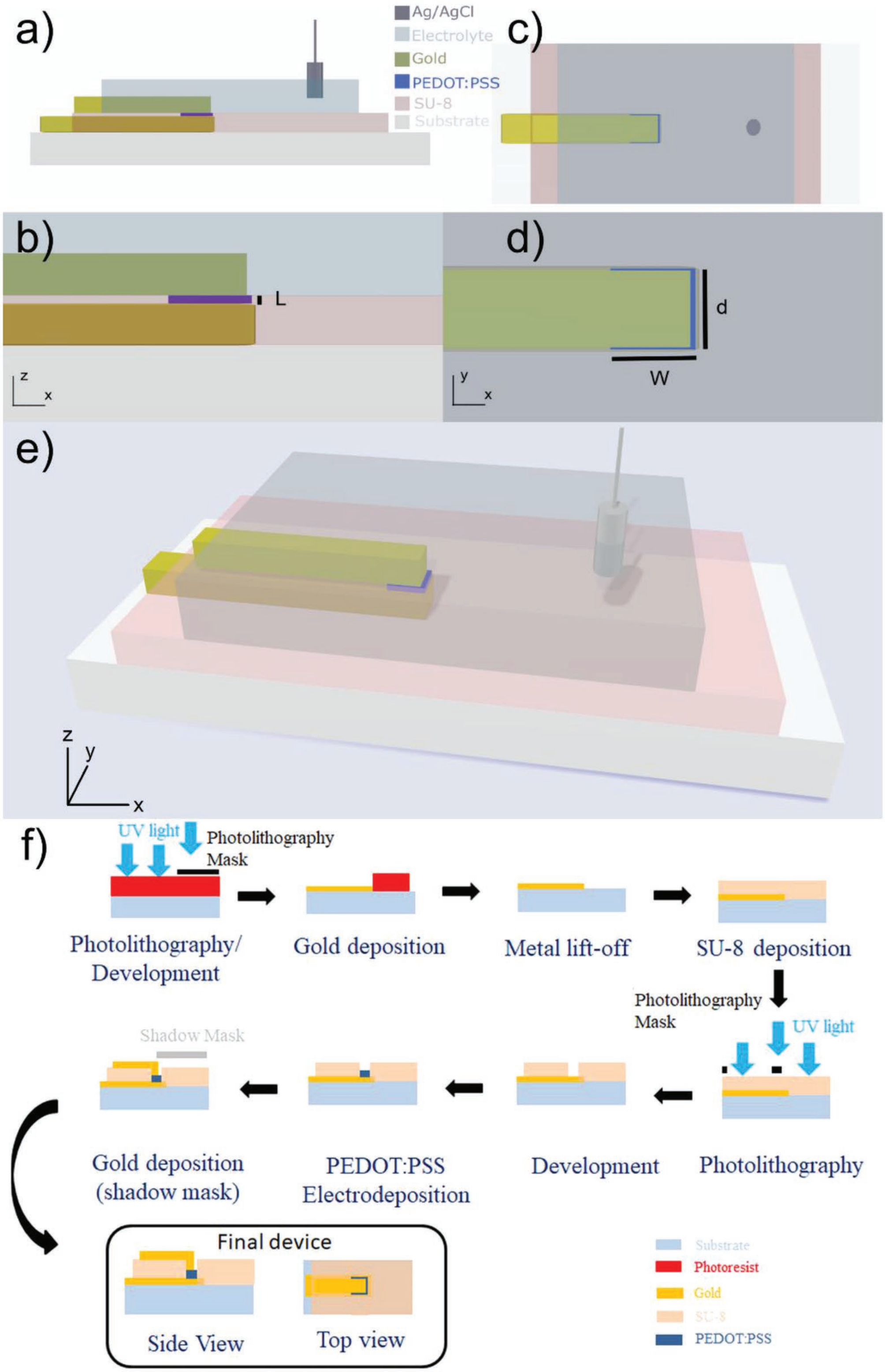

Figure 1. Schematic representation of the device geometry (not to scale). a) Side view of the vOECT topology. The device is realized with deposition of consecutive layers of gold, PEDOT:PSS and gold, one on top of the other. An Ag/AgCl electrode serves as the device gate. SU-8 is used for the encapsulation. Specifically, it prevents the direct contact between the source electrode and the electrolyte as well as insulates the source-drain connection tracks. b) A zoom in on (a). The channel length (*L*) is defined by the thickness of the PEDOT:PSS film. c) Top view of the vertical transistor. d) A zoom in on (c). An intentional top electrode misalignment, assist the polymer de-doping during the device operation. e) A graphical projection of the device. f) Schematic of the fabrication method.

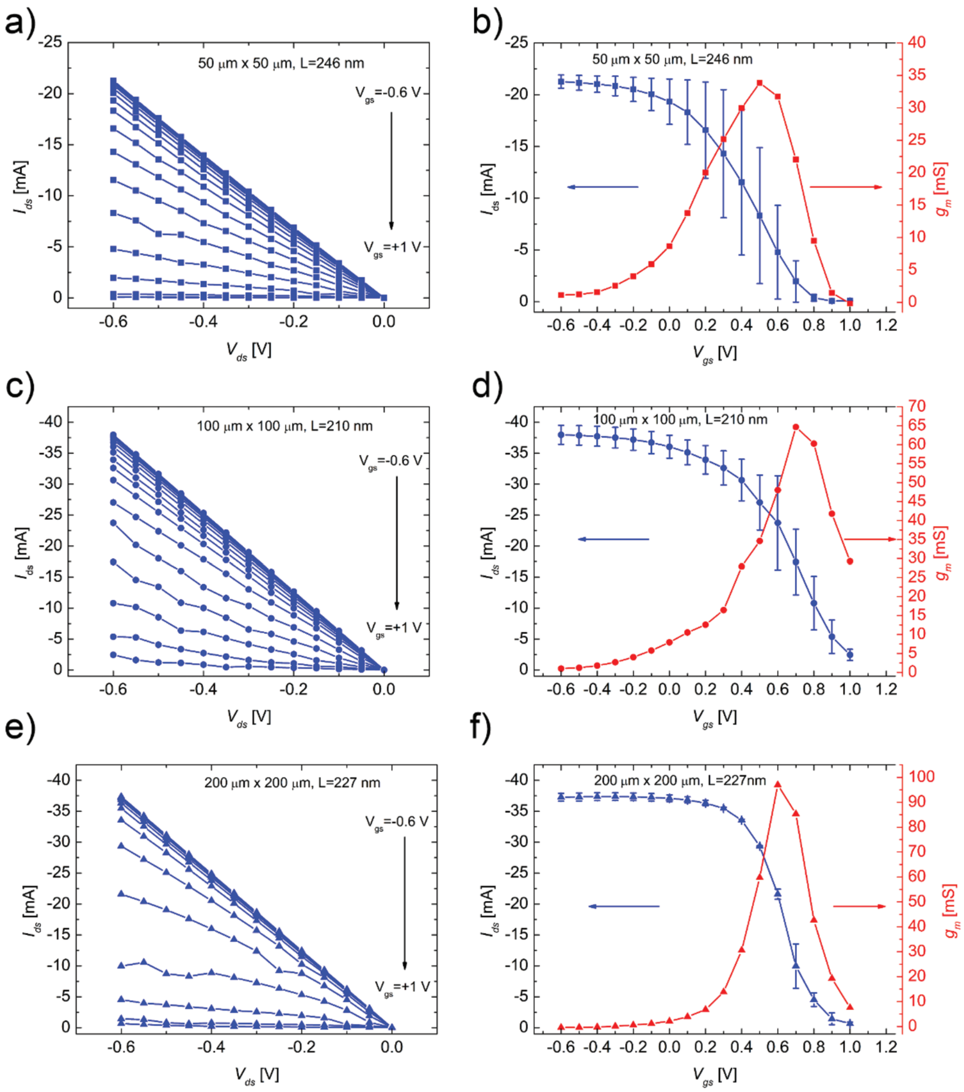

Figure 2. Electrical characterization of the vertical channel organic electrochemical transistors for various device geometries $W \times d$. a) Output curves of a 50 µm × 50 µm ($W \times d$) device with channel length $L = 246$ nm. b) Transfer curve and the corresponding transconductance of the same device. The increased product $W \times d$ and the sub-micrometer channel length result in a maximum transconductance of about 34 mS. c,d) Output curves, transfer curve, and transconductance of a 100 µm × 100 µm ($W \times d$) device with a channel length $L = 210$ nm. The increase of the product $W \times d$ results in a maximum transconductance of about 65 mS. e,f) Output curves, transfer curve, and transconductance of a 200 µm × 200 µm ($W \times d$) device of a similar channel length ($L = 227$ nm). The increased $W \times d$ product results in a maximum transconductance of about 97 mS. All measurements were carried out in 0.1 M NaCl. For the output curves, the drain voltage sweeps from 0 to –0.6 V with a –0.05 V voltage step and the gate voltage from –0.6 V to +1 V with a +0.1 V voltage step. The transfer curve is presented for $V_{ds} = -0.6$ V. The transconductance was calculated for $V_{ds} = -0.6$ V. The plots show the mean values of three measurements ($n = 3$). The error bars represent the standard deviation of the dataset.

before as a short channel effect for short channel organic field effect transistors.[25]

To further investigate the transconductance limits, we studied the effect of the channel geometry in the operational figures of merit, as shown in **Figure 3**.

It is already known that the channel length (L) affects the transistor's performance. In particular, shorter channels result in higher transconductance values, increased channel currents, and higher transition frequencies.[26] Therefore, we expected that a change in the vertical transistor channel length would be mirrored in its figures of merit. First, the OECT's channel length (L) was increased to 397 nm for the 100 µm × 100 µm ($W \times d$) footprint. The device electrical characteristics are presented in Figure 3a,b. As expected, the maximum channel current decreased compared with the device presented in Figure 2c,d, which has the same $W \times d$. On the contrary, a decrease of the channel length is expected to increase the transistor current and its transconductance. Since g_m is affected by the overall channel geometry, an increase of the area $W \times d$ combined with a simultaneous reduction of L would result in high channel currents and high transconductance values. Figure 3c presents the output curves of a 500 µm × 500 µm ($W \times d$) vOECT with channel length $L = 59$ nm, which can support currents up to 115 mA. The maximum transconductance is as high

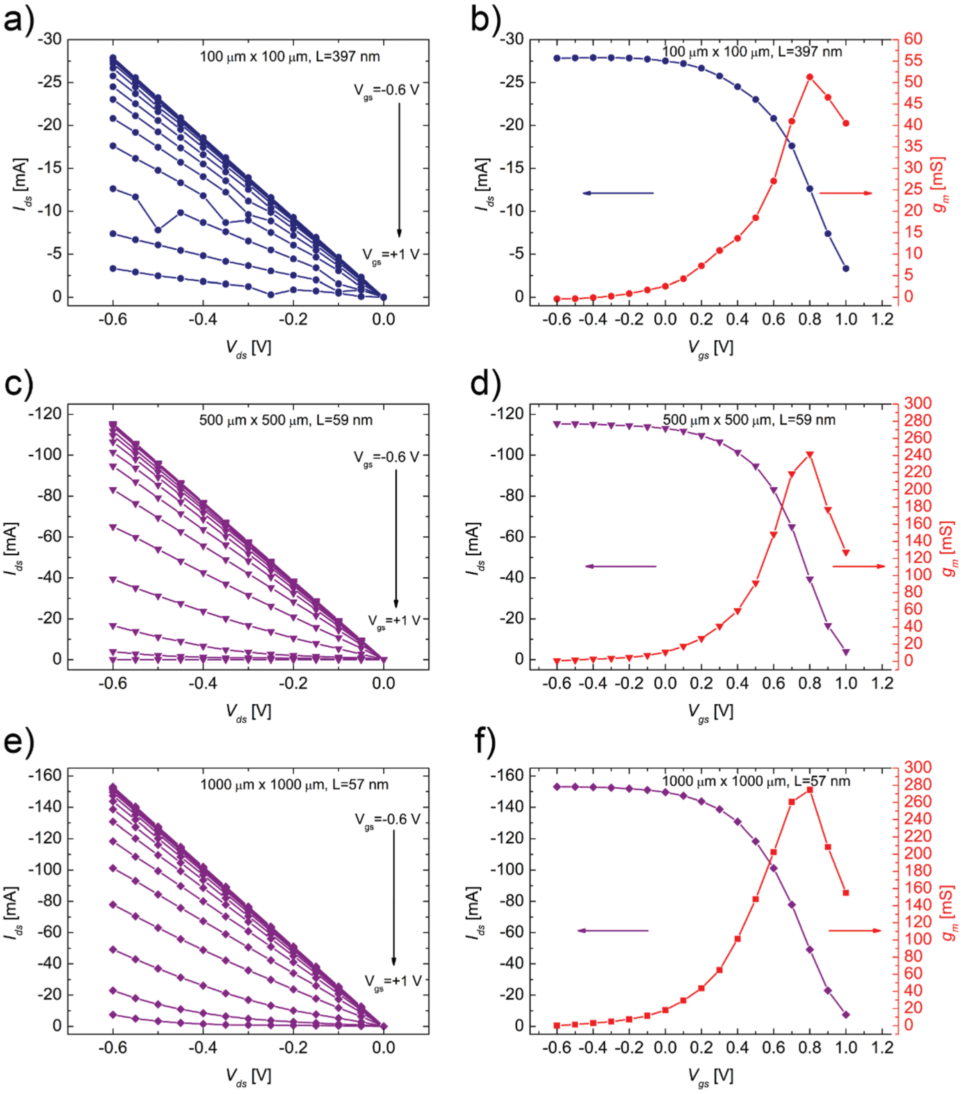

Figure 3. Effect of the channel geometry on the electrical characteristics of the device. a,b) Output curves, transfer curve, and transconductance of a 100 µm × 100 µm ($W \times d$) device with channel length $L = 397$ nm. The increased channel length, compared with the one of the device in Figure 2c,d, which has the same $W \times d$, is echoed both in the reduced maximum device current and the lower transconductance. c,d) Output curves, transfer curve, and transconductance of a 500 µm × 500 µm ($W \times d$) device with channel length $L = 59$ nm. The increased device footprint and the decreased channel length result in an extremely high maximum transconductance of about 242 mS. e,f) Output curves, transfer curve, and transconductance of a 1000 µm × 1000 µm ($W \times d$) device with channel length $L = 57$ nm. The large device footprint ($W \times d$) and the submicron channel deliver 275 mS of transconductance. For the output curves, the drain voltage sweeps from 0 to –0.6 V with a –0.05 V voltage step and the gate voltage from –0.6 V to +1 V with a +0.1 V voltage step. The transfer curve is presented for $V_{ds} = -0.6$ V. The transconductance was calculated for $V_{ds} = -0.6$ V. The steady state gate current for $V_{ds} = -0.6$ V of the devices is presented in Figure S6 (Supporting Information). All measurements were carried out in 0.1 м NaCl.

as 242 mS (Figure 3d). To push the device limits even further, we fabricated a device with $W \times d = 1000$ µm × 1000 µm and channel length $L = 57$ nm. This vOECT supports currents of up to 150 mA as shown in the output curves of Figure 3e, while its transfer curve and its transconductance are presented in Figure 3f. It is worth mentioning that the obtained transconductance value g_m of 275 mS is, to the best of our knowledge, the highest one reported up to date.

It should be noted that the above unprecedently high transconductance value is achieved with a PEDOT:PSS film channel, which was electrodeposited from EDOT and PSS without the addition of any of the conductivity enhancers that are typically used in the literature, such as ethylene glycol (EG) or dimethyl sulfoxide (DMSO).[27] Therefore, it can be speculated that these values can be increased even further if the conducting polymer film would be additionally treated with an appropriate solvent.

To further investigate the relation between transconductance and the OECT geometry, we evaluated the scaling with Wd/L and the results are presented in **Figure 4**a.

During the fabrication of the vertical OECTs, special care was taken to the parasitic resistances induced by the tracks connecting the devices. In particular, the designed vOECT contact lines were wide, with short length and a thickness of

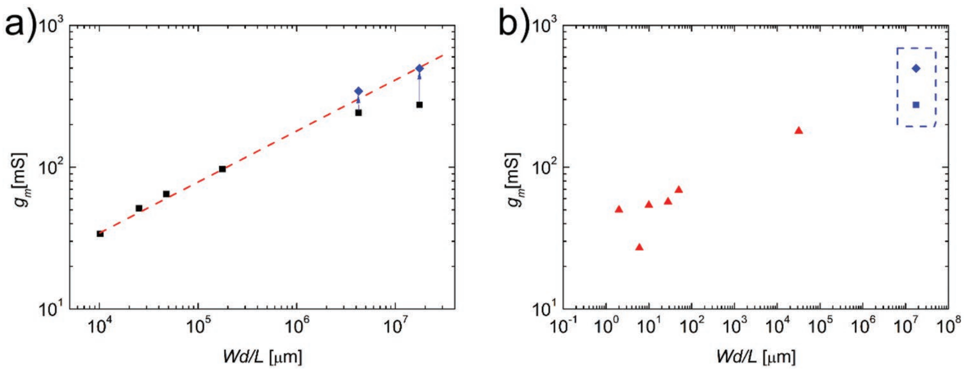

Figure 4. a) Scaling of vertical OECT transconductance with device geometry. For large $W \times d$ values and small channel lengths (L), the transistor lead resistance becomes comparable to the channel resistance and the transconductance values start to saturate. After correcting for the resistance of the connecting tracks, the obtained intrinsic transconductance g_{mi} (shown in blue diamonds) agrees with the theoretically expected one. The dashed red line is a guide to the eye. b) The highest obtained transconductance of this work is benchmarked against the highest reported transconductance values in the literature (red triangles).[19,22,28] The blue square indicates the measured g_{m} and the blue diamond the intrinsic one g_{mi} for the best performing device ($W \times d$ = 1000 µm × 1000 µm, d = 57 nm). The values of this work are shown inside the blue rectangle.

200 nm (a value twice the one typically used in OECTs). The above fabrication parameters ensured a track resistance lower than the channel resistance up to a minimum channel length of ≈210 nm. However, for vOECTs with large $W \times d$ footprints (500 µm × 500 µm and 1000 µm × 1000 µm) and very short channels (≈60 nm) the lead resistance became significant and, as a result, the transconductance in Figure 4a saturates. This has been addressed before with the calculation of the intrinsic (g_{mi}) transconductance as opposed to the measured one g_{m}.[19,29] Especially, for short channels with low channel resistance and high transconductance values, the measured transconductance is much lower than the intrinsic one, due to the parasitic source-drain series resistance R_{SD}. The intrinsic transconductance can be calculated as follows:

$$g_{\mathrm{mi}} = \frac{g_{\mathrm{m}}^{0}}{\left(1 - R_{\mathrm{SD}} g_{\mathrm{D}} \left(1 + R_{\mathrm{s}} g_{\mathrm{m}}^{0}\right)\right)} \tag{1}$$

where $g_{\mathrm{D}} = \frac{\partial I_{\mathrm{DS}}}{\partial V_{\mathrm{DS}}}$ is the output conductance, R_{SD} the drain-source series resistance, R_{s} the source series resistance, and g_{m}^{0} reads:

$$g_{\mathrm{m}}^{0} = \frac{g_{\mathrm{m}}}{\left(1 - R_{\mathrm{s}} g_{\mathrm{m}}\right)} \tag{2}$$

where g_{m} is the measured transconductance.

The R_{s} and R_{SD}were measured to be in the order of a few ohms for the vOECTs of Figure 3 and their drain conductance was calculated from the output curves at $V_{\mathrm{ds}} = -0.6$ V, viz. the drain bias used for the transconductance calculation. The calculated intrinsic transconductance g_{mi} is plotted in Figure 4a (blue diamonds). Remarkably, these values are positioned exactly on the expected values of the trend line. It should also be pointed out that the calculated intrinsic transconductance for the device with the largest footprint $W \times d$ (1000 µm × 1000 µm) and shortest channel (57 nm), results in an extraordinary value of 498 mS. In Figure 4b, this value is benchmarked against the highest reported values of other state-of-the-art devices, highlighting the advantage of our proposed fabrication approach.

3. Conclusion

In summary, a vertical channel organic electrochemical transistor (vOECT) is presented with ultrashort PEDOT:PSS channel, sandwiched between two (bottom and top) gold electrodes. This architecture takes advantage of the third dimension, which is perpendicular to the substrate. The proposed fabrication process allows for an accurate control of the transistor $W \times d$ product via a simple photolithography step. This is critical, as $W \times d$ can now be set to very high values. At the same time, the transistor channel is precisely defined by the organic polymer thickness, through an electrodeposition step. This is also significant, as it allows for the realization of OECTs with vertical channels below 100 nm. Combination of the above features results in an unprecedented high transconductance of 275 mS, unattainable with conventional planar OECTs. Due to the very high currents, the transconductance is limited by the voltage drop over the connection tracks. The intrinsic transconductance g_{mi} after correction for the parasitic voltage drop amounts to 498 mS. It is also noteworthy that the ultrahigh transconductance value stems exclusively from the new device architecture, since the conducting polymer film conductivity is not enhanced by any solvent treatment. Therefore, this work reports a new class of high-performing three-dimensional OECTs, which offer new pathways for bioelectronic applications.

4. Experimental Section

Fabrication: The device fabrication was realized with standard microfabrication methods. First, the device substrate (optical microscope glass slides—26 mm × 76 mm) was thoroughly cleaned in a soap (1% vol vol^{-1}, Micro-90) and then in a solvent mixture (acetone/isopropanol, 1:1) bath. Subsequently, a photolithography step (used photoresist: S 1813) was employed for the gold bottom electrode patterning. Gold of 200 nm of thickness (with a 10 nm Cr layer initially deposited, to promote the gold adhesion on the substrate) was first sputtered on top of the S 1813 and a lift-off step in a solvent mixture (acetone/isopropanol, 1:1) resulted in the designed bottom electrode. The electrode was optimized in length, width, and thickness. Then, a negative epoxy-based photoresist (SU-8) was used to encapsulate the electrode, while an exposure and a following development step defined openings on the connection pad and on the electrode tip. The SU-8 opening on the electrode tip defined the vOECT channel width (*W*) and thickness (*d*). Next, the PEDOT:PSS film was electropolymerized inside the SU-8 opening and on the gold electrode tip, from EDOT and PSS in deionized water. This step defined the transistor channel length (*L*). The volumetric capacitance of PEDOT:PSS, namely 39 F cm^{-3},[13] was used for the calculation of the OECT channel length (*L*), since the width (*W*) and thickness (*d*) were already set through the microfabrication process (Figure S3 and Table S1, Supporting Information). Finally, the transistor top electrode was deposited via gold sputtering (200 nm Au thickness, no Cr adhesion layer) through a shadow mask (Pfeiffer-vacuum sputtering system), to conclude the vertical channel OECT structure.

Electropolymerization: The poly(3,4-ethylenedioxythiophene) polystyrene sulfonate (PEDOT:PSS) transistor channel was formed through an oxidative electrochemical-driven reaction as previously reported.[30] The 3,4-ethylenedioxythiophen (EDOT) monomers were electrochemically polymerized to PEDOT:PSS from an aqueous solution that also contained poly(sodium4-styrene sulfonate) (PSSNa) in a ratio 1:10 (0.01 M EDOT/0.1 M PSSNa). A steady current (galvanostatic mode) provided the required energy for the reaction and the resulting film formation.[4]

SU-8 photoresist deposition: The photoresist SU-8 was used to electrically insulate the bottom electrode and to define the $W \times d$ of the channel. SU-8 was spin coated on the devices and was baked at 65 °C for 45 min and at 95 °C for 2 min before the exposure. After the exposure, consecutive baking steps at 65 °C–95 °C–65 °C for 1 min and a development step concluded the SU-8 patterning.

Electrical Characterization and Measurements: A polydimethylsiloxane (PDMS) well was attached on the device active area in order to host the employed electrolyte. The well was filled with NaCl solution (0.1 M). A potentiostat (PlamSens4) was used for the impedance spectroscopy measurements in a three-electrode configuration. The transistor source and drain were shorted and used as the working electrode. An Ag/AgCl and a Pt electrode served as the reference and the counter electrode respectively. The transistors output and transfer curves were obtained with a dual channel Keithley 2600 SMU.

Data Analysis: The recorded data were analyzed, modeled, and plotted with the help of Python, EIS Spectrum Analyser, and Origin Ltd softwares. Figures 2 and 4 report mean values of current and transconductance of three measurements ($n = 3$). For Figure 2a,b, $n = 2$. The error bars in the plots represent the standard deviation of the data set.

Supporting Information

Supporting Information is available from the Wiley Online Library or from the author.

Acknowledgements

((Acknowledgements, general annotations, funding. Other references to the title/authors can also appear here, such as "Author 1 and Author 2 contributed equally to this work."))

Open access funding enabled and organized by Projekt DEAL.

Conflict of Interest

The authors declare no conflict of interest.

Data Availability Statement

The data that support the findings of this study are available from the corresponding author upon reasonable request.

Keywords

3D bioelectronic devices, device physics, implantable devices, organic electrochemical transistors, organ-on-a-chip

Received: August 9, 2022
Revised: October 24, 2022
Published online: November 22, 2022

---

[1] a) E. Zeglio, A. L. Rutz, T. E. Winkler, G. G. Malliaras, A. Herland, *Adv. Mater.* **2019**, *31*, 1806712; b) D. Ohayon, S. Inal, *Adv. Mater.* **2020**, *32*, 2001439.

[2] T. Someya, Z. Bao, G. G. Malliaras, *Nature* **2016**, *540*, 379.

[3] J. Rivnay, R. M. Owens, G. G. Malliaras, *Chem. Mater.* **2014**, *26*, 679.

[4] X. Cui, D. C. Martin, *Sens. Actuators, B* **2003**, *89*, 92.

[5] a) D. A. Koutsouras, A. Hama, J. Pas, P. Gkoupidenis, B. Hivert, C. Faivre-Sarrailh, E. Di Pasquale, R. M. Owens, G. G. Malliaras, *MRS Commun.* **2017**, *7*, 259; b) D. Khodagholy, J. N. Gelinas, T. Thesen, W. Doyle, O. Devinsky, G. G. Malliaras, G. Buzsáki, *Nat. Neurosci.* **2015**, *18*, 310; c) J. Pas, C. Pitsalidis, D. A. Koutsouras, P. P. Quilichini, F. Santoro, B. Cui, L. Gallais, R. P. O'Connor, G. G. Malliaras, R. M. Owens, *Adv. Biosyst.* **2018**, *2*, 1700164; d) R. A. Green, N. H. Lovell, G. G. Wallace, L. A. Poole-Warren, *Biomaterials* **2008**, *29*, 3393; e) G. D. Spyropoulos, J. Savarin, E. F. Gomez, D. T. Simon, M. Berggren, J. N. Gelinas, E. Stavrinidou, D. Khodagholy, *Adv. Mater. Technol.* **2020**, *5*, 1900652.

[6] D. A. Koutsouras, R. Perrier, A. Villarroel Marquez, A. Pirog, E. Pedraza, E. Cloutet, S. Renaud, M. Raoux, G. G. Malliaras, J. Lang, *Mater. Sci. Eng. C Mater. Biol. Appl.* **2017**, *81*, 84.

[7] a) G. Dijk, H. J. Ruigrok, R. P. O'Connor, *Adv. Mater. Interfaces* **2021**, *8*, 2100214; b) N. Rossetti, J. E. Hagler, P. Kateb, F. Cicoira, *J. Mater. Chem. C* **2021**, *9*, 7243.

[8] D. A. Koutsouras, L. V. Lingstedt, K. Lieberth, J. Reinholz, V. Mailänder, P. W. M. Blom, P. Gkoupidenis, *Adv. Healthcare Mater.* **2019**, *8*, 1901215.

[9] a) R. M. Owens, G. G. Malliaras, *MRS Bull.* **2010**, *35*, 449; b) C. Pitsalidis, A.-M. Pappa, A. J. Boys, Y. Fu, C.-M. Moysidou, D. van Niekerk, J. Saez, A. Savva, D. Iandolo, R. M. Owens, *Chem. Rev.* **2022**, *122*, 4700.

[10] a) F. Torricelli, D. Z. Adrahtas, Z. Bao, M. Berggren, F. Biscarini, A. Bonfiglio, C. A. Bortolotti, C. D. Frisbie, E. Macchia, G. G. Malliaras, I. McCulloch, M. Moser, T.-Q. Nguyen, R. M. Owens, A. Salleo, A. Spanu, L. Torsi, *Nat. Rev. Methods Primers* **2021**, *1*, 66; b) F. Leonardi, S. Casalini, Q. Zhang, S. Galindo, D. Gutiérrez, M. Mas-Torrent, *Adv. Mater.* **2016**, *28*, 10311; c) R. F. de Oliveira, S. Casalini, T. Cramer, F. Leonardi, M. Ferreira, V. Vinciguerra, V. Casuscelli, N. Alves, M. Murgia, L. Occhipinti, F. Biscarini, *Flex. Print. Electron.* **2016**, *1*, 025005.

[11] a) D. A. Bernards, G. G. Malliaras, *Adv. Funct. Mater.* **2007**, *17*, 3538; b) D. A. Koutsouras, P. Leleux, M. Ramuz, J. Rivnay, G. G. Malliaras, presented at *2014 IEEE International Electron Devices Meet.*, IEEE, San Francisco, CA, USA December **2014**; c) J. Rivnay, S. Inal, A. Salleo, R. M. Owens, M. Berggren, G. G. Malliaras, *Nat. Rev. Mater.* **2018**, *3*, 17086.

[12] a) D. Khodagholy, T. Doublet, P. Quilichini, M. Gurfinkel, P. Leleux, A. Ghestem, E. Ismailova, T. Hervé, S. Sanaur, C. Bernard, G. G. Malliaras, *Nat. Commun.* **2013**, *4*, 1575; b) Y. Liang, M. Ernst, F. Brings, D. Kireev, V. Maybeck, A. Offenhäusser, D. Mayer, *Adv. Healthcare Mater.* **2018**, *7*, 1800304; c) C. Cea, G. D. Spyropoulos, P. Jastrzebska-Perfect, J. J. Ferrero, J. N. Gelinas, D. Khodagholy, *Nat. Mater.* **2020**, *19*, 679.

[13] J. Rivnay, P. Leleux, M. Ferro, M. Sessolo, A. Williamson, D. A. Koutsouras, D. Khodagholy, M. Ramuz, X. Strakosas,

R. M. Owens, C. Benar, J.-M. Badier, C. Bernard, G. G. Malliaras, *Sci. Adv.* **2015**, *1*, e1400251.
[14] a) L. H. Jimison, S. A. Tria, D. Khodagholy, M. Gurfinkel, E. Lanzarini, A. Hama, G. G. Malliaras, R. M. Owens, *Adv. Mater.* **2012**, *24*, 5919; b) P. Romele, P. Gkoupidenis, D. A. Koutsouras, K. Lieberth, Z. M. Kovács-Vajna, P. W. M. Blom, F. Torricelli, *Nat. Commun.* **2020**, *11*, 3743; c) K. Lieberth, P. Romele, F. Torricelli, D. A. Koutsouras, M. Brückner, V. Mailänder, P. Gkoupidenis, P. W. M. Blom, *Adv. Healthcare Mater.* **2021**, *10*, 2100845; d) A.-M. Pappa, H.-Y. Liu, W. Traberg-Christensen, Q. Thiburce, A. Savva, A. Pavia, A. Salleo, S. Daniel, R. M. Owens, *ACS Nano* **2020**, *14*, 12538; e) K. Guo, S. Wustoni, A. Koklu, E. Díaz-Galicia, M. Moser, A. Hama, A. A. Alqahtani, A. N. Ahmad, F. S. Alhamlan, M. Shuaib, A. Pain, I. McCulloch, S. T. Arold, R. Grünberg, S. Inal, *Nat. Biomed. Eng.* **2021**, *5*, 666.
[15] a) M. Ghittorelli, L. Lingstedt, P. Romele, N. I. Crăciun, Z. M. Kovács-Vajna, P. W. M. Blom, F. Torricelli, *Nat. Commun.* **2018**, *9*, 1441; b) S. Han, S. Yamamoto, A. G. Polyravas, G. G. Malliaras, *Adv. Mater.* **2020**, *32*, 2004790; c) D. A. Koutsouras, K. Lieberth, F. Torricelli, P. Gkoupidenis, P. W. M. Blom, *Adv. Mater. Technol.* **2021**, *6*, 2100591.
[16] a) G. Tarabella, P. D'Angelo, A. Cifarelli, A. Dimonte, A. Romeo, T. Berzina, V. Erokhin, S. Iannotta, *Chem. Sci.* **2015**, *6*, 2859; b) Y. van de Burgt, E. Lubberman, E. J. Fuller, S. T. Keene, G. C. Faria, S. Agarwal, M. J. Marinella, A. Alec Talin, A. Salleo, *Nat. Mater.* **2017**, *16*, 414; c) P. C. Harikesh, C.-Y. Yang, D. Tu, J. Y. Gerasimov, A. M. Dar, A. Armada-Moreira, M. Massetti, R. Kroon, D. Bliman, R. Olsson, E. Stavrinidou, M. Berggren, S. Fabiano, *Nat. Commun.* **2022**, *13*, 901; d) C. Lubrano, U. Bruno, C. Ausilio, F. Santoro, *Adv. Mater.* **2022**, *34*, 2110194.
[17] J. T. Mabeck, G. G. Malliaras, *Anal. Bioanal. Chem.* **2006**, *384*, 343.
[18] a) N. Stutzmann, R. H. Friend, H. Sirringhaus, *Science* **2003**, *299*, 1881; b) R. Parashkov, E. Becker, S. Hartmann, G. Ginev, D. Schneider, H. Krautwald, T. Dobbertin, D. Metzdorf, F. Brunetti, C. Schildknecht, A. Kammoun, M. Brandes, T. Riedl, H.-H. Johannes, W. Kowalsky, *Appl. Phys. Lett.* **2003**, *82*, 4579; c) R. Parashkov, E. Becker, S. Hartmann, G. Ginev, D. Schneider, H. Krautwald, T. Dobbertin, D. Metzdorf, F. Brunetti, C. Schildknecht, A. Kammoun, M. Brandes, T. Riedl, H.-H. Johannes, W. Kowalsky, *Appl. Phys. Lett.* **2004**, *84*, 157; d) M. Uno, Y. Tominari, J. Takeya, *Appl. Phys. Lett.* **2008**, *93*, 173301; e) F. Kaschura, A. Fischer, D. Kasemann, K. Leo, B. Lüssem, *Appl. Phys. Lett.* **2015**, *107*, 033301; f) A. A. Günther, C. Hossbach, M. Sawatzki, D. Kasemann, J. W. Bartha, K. Leo, *Appl. Phys. Lett.* **2015**, *107*, 233302.
[19] M. J. Donahue, A. Williamson, X. Strakosas, J. T. Friedlein, R. R. McLeod, H. Gleskova, G. G. Malliaras, *Adv. Mater.* **2018**, *30*, 1705031.
[20] a) R. B. Rashid, W. Du, S. Griggs, I. P. Maria, I. McCulloch, J. Rivnay, *Sci. Adv.* **2021**, *7*, eabh1055; b) M. Abarkan, A. Pirog, D. Mafilaza, G. Pathak, G. N'Kaoua, E. Puginier, R. O'Connor, M. Raoux, M. J. Donahue, S. Renaud, J. Lang, *Adv. Sci.* **2022**, *9*, 2105211.
[21] J. Lenz, F. Del Giudice, F. R. Geisenhof, F. Winterer, R. T. Weitz, *Nat. Nanotechnol.* **2019**, *14*, 579.
[22] Y. Yan, Q. Chen, X. Wang, Y. Liu, R. Yu, C. Gao, H. Chen, T. Guo, *ACS Appl. Mater. Interfaces* **2021**, *13*, 7498.
[23] F. Torricelli, L. Colalongo, D. Raiteri, Z. M. Kovács-Vajna, E. Cantatore, *Nat. Commun.* **2016**, *7*, 10550.
[24] Y. Choi, S. Oh, C. Qian, J.-H. Park, J. H. Cho, *Nat. Commun.* **2020**, *11*, 4595.
[25] J. N. Haddock, X. Zhang, S. Zheng, Q. Zhang, S. R. Marder, B. Kippelen, *Org. Electron.* **2006**, *7*, 45.
[26] H. Kleemann, K. Krechan, A. Fischer, K. Leo, *Adv. Funct. Mater.* **2020**, *30*, 1907113.
[27] a) L. V. Lingstedt, M. Ghittorelli, H. Lu, D. A. Koutsouras, T. Marszalek, F. Torricelli, N. I. Crăciun, P. Gkoupidenis, P. W. M. Blom, *Adv. Electron. Mater.* **2019**, *5*, 1800804; b) H. Shi, C. Liu, Q. Jiang, J. Xu, *Adv. Electron. Mater.* **2015**, *1*, 1500017.
[28] a) V. Venkatraman, J. T. Friedlein, A. Giovannitti, I. P. Maria, I. McCulloch, R. R. McLeod, J. Rivnay, *Adv. Sci. (Weinh.)* **2018**, *5*, 1800453; b) J. Ko, X. Wu, A. Surendran, B. T. Muhammad, W. L. Leong, *ACS Appl. Mater. Interfaces* **2020**, *12*, 33979; c) L. Wang, Q. Sun, L. Zhang, J. Wang, G. Ren, L. Yu, K. Wang, Y. Zhu, G. Lu, H.-D. Yu, *Macromol. Rapid Commun.* **2022**, *43*, 2200212.
[29] S. Y. Chou, D. A. Antoniadis, *IEEE Trans. Electron Devices* **1987**, *34*, 448.
[30] D. A. Koutsouras, F. Torricelli, P. Gkoupidenis, P. W. M. Blom, *Adv. Mater. Technol.* **2021**, *6*, 2100732.

ADVANCED
ELECTRONIC
MATERIALS

Supporting Information

for *Adv. Electron. Mater.,* DOI: 10.1002/aelm.202200868

Submicron Vertical Channel Organic Electrochemical Transistors with Ultrahigh Transconductance

Dimitrios A. Koutsouras, Fabrizio Torricelli, and Paul W.M. Blom**

Supporting Information

Submicron Vertical Channel Organic Electrochemical Transistors with Ultra-High Transconductance

Dimitrios A. Koutsouras, Fabrizio Torricelli and Paul W.M. Blom**

Figure S1: Optical micrographs of the vertical channel OECTs.

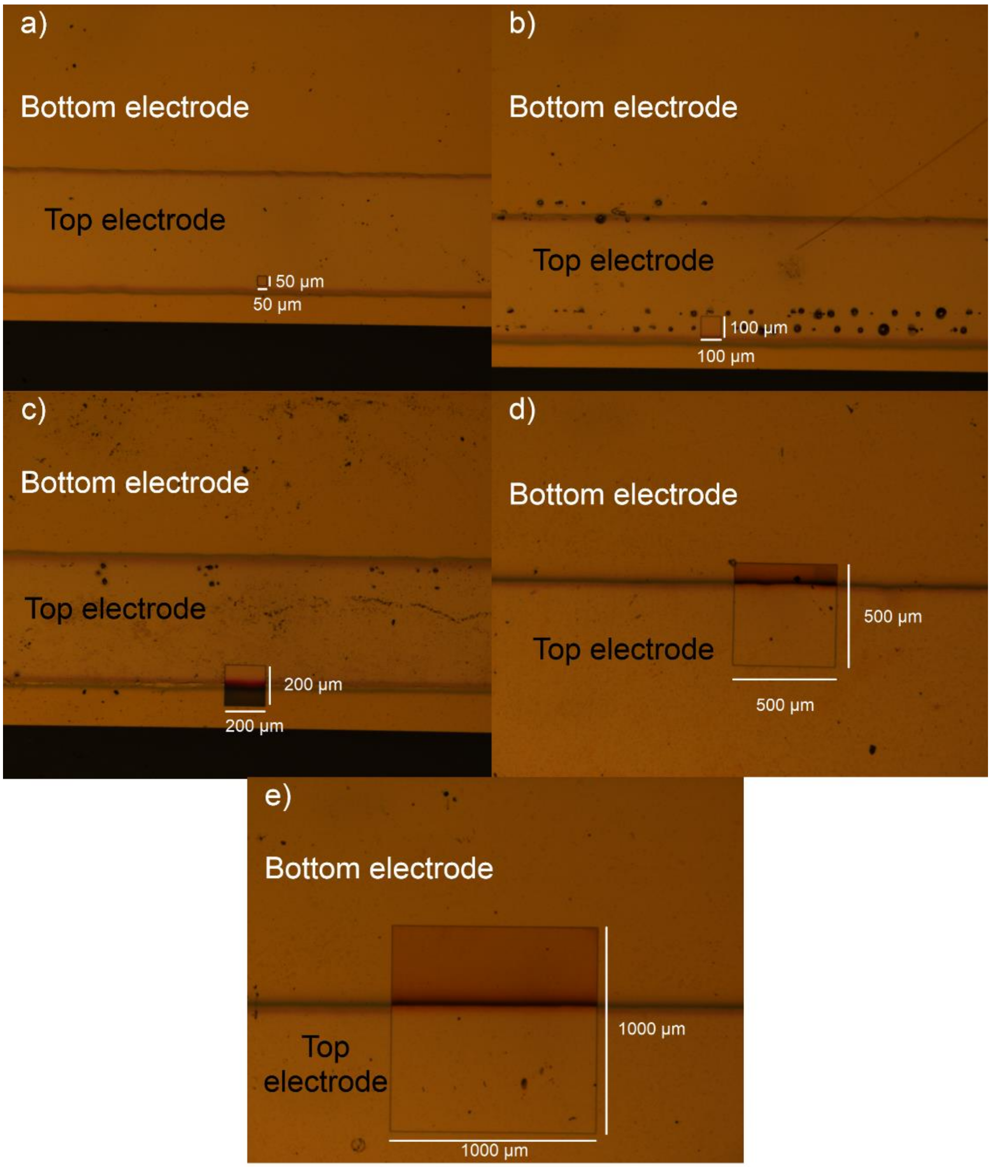

Figure S1: a-e) Optical micrographs of the vertical channel OECTs: The channel's wxd footprint is a square with dimensions increasing from 50 µm x 50 µm to 1000 µm x1000 µm. a) 50 µm x 50 µm (*W*×*d*), *L*= 246 nm b) 100 µm x 100 µm (*W*×*d*), *L*= 210 nm c) 200 µm x 200 µm (*W*×*d*), *L*= 227 nm d) 500 µm x 500 µm (*W*×*d*), *L*=59 nm e) 1000 µm x 1000 µm, *L*=57 nm.

Figure S2: Electrochemical characterization of the submicron vertical channel OECTs. Figure S1 presents the impedance spectra of the vOECT channels. Fitting of the impedance spectra with an equivalent R-C circuit results in the values of the capacitance C_{ch} of the transistor channel. The C_{ch} of the channel is used for the calculation of the channel length L through the PEDOT:PSS volumetric capacitance value (39 F/cm^3) (Table S1).

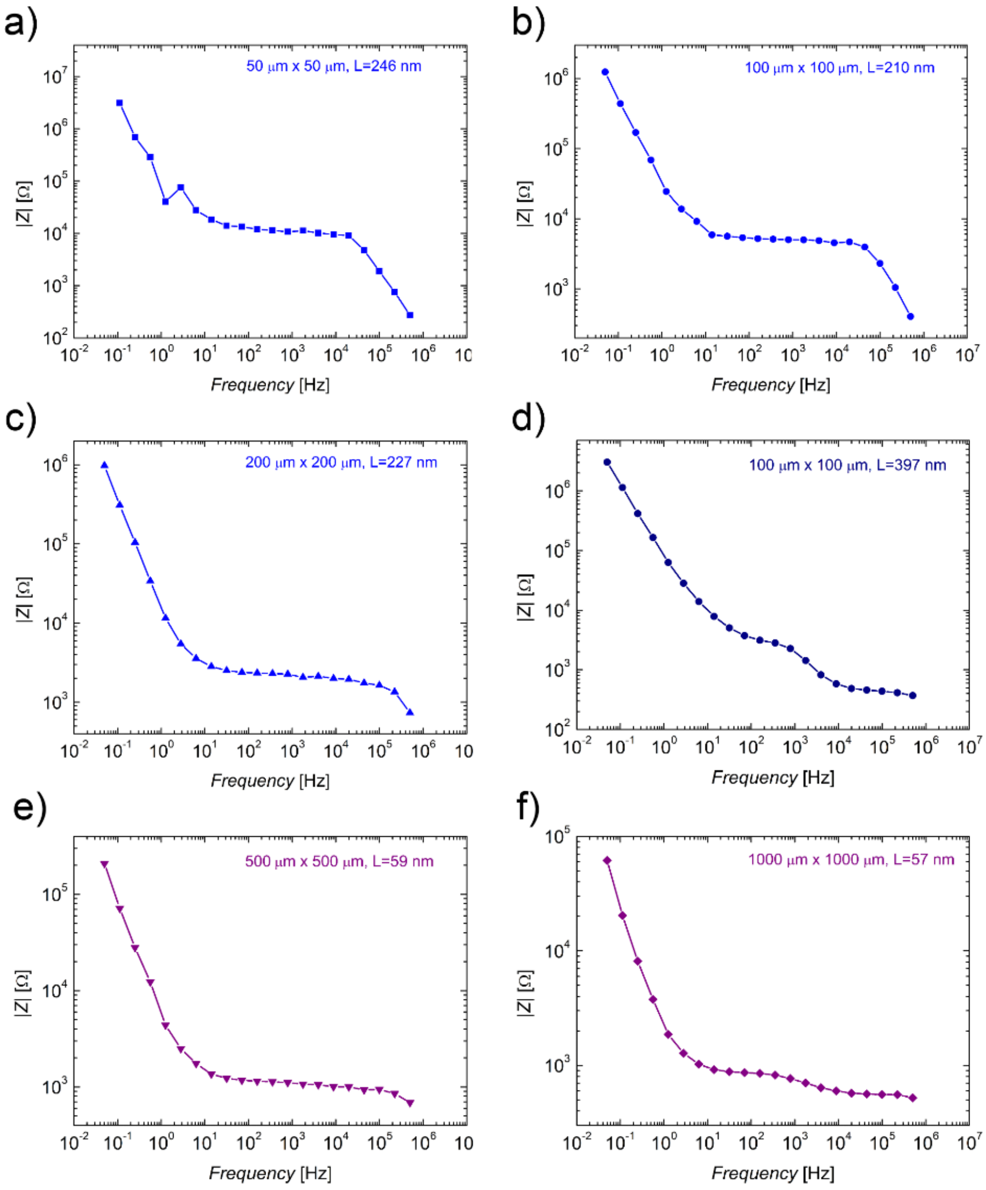

Figure S2: Electrochemical impedance spectroscopy of the channels of the vOECTs. a,b,c) The $W\times d$ product increases from 50 μm x 50 μm, to 100 μm x 100 μm and finally to 200 μm x 200 μm, while the channel length is around 230 nm. d) Impedance spectrum of the $W\times d$ =100 μm x 100 μm transistor. The channel length is L=397 nm. e,f) Impedance spectra of sub 100nm channel vOECTs. The channel length is around 60 nm for two $W\times d$ values, 500 μm x 500 μm and 1000 μm x 1000 μm respectively.

Figure S3: Fitting of the impedance spectra data of Figure S2 with a R-C equivalent model. The obtained values are reported in Table S1. The EIS Spectrum Analyser software was used for the fitting.

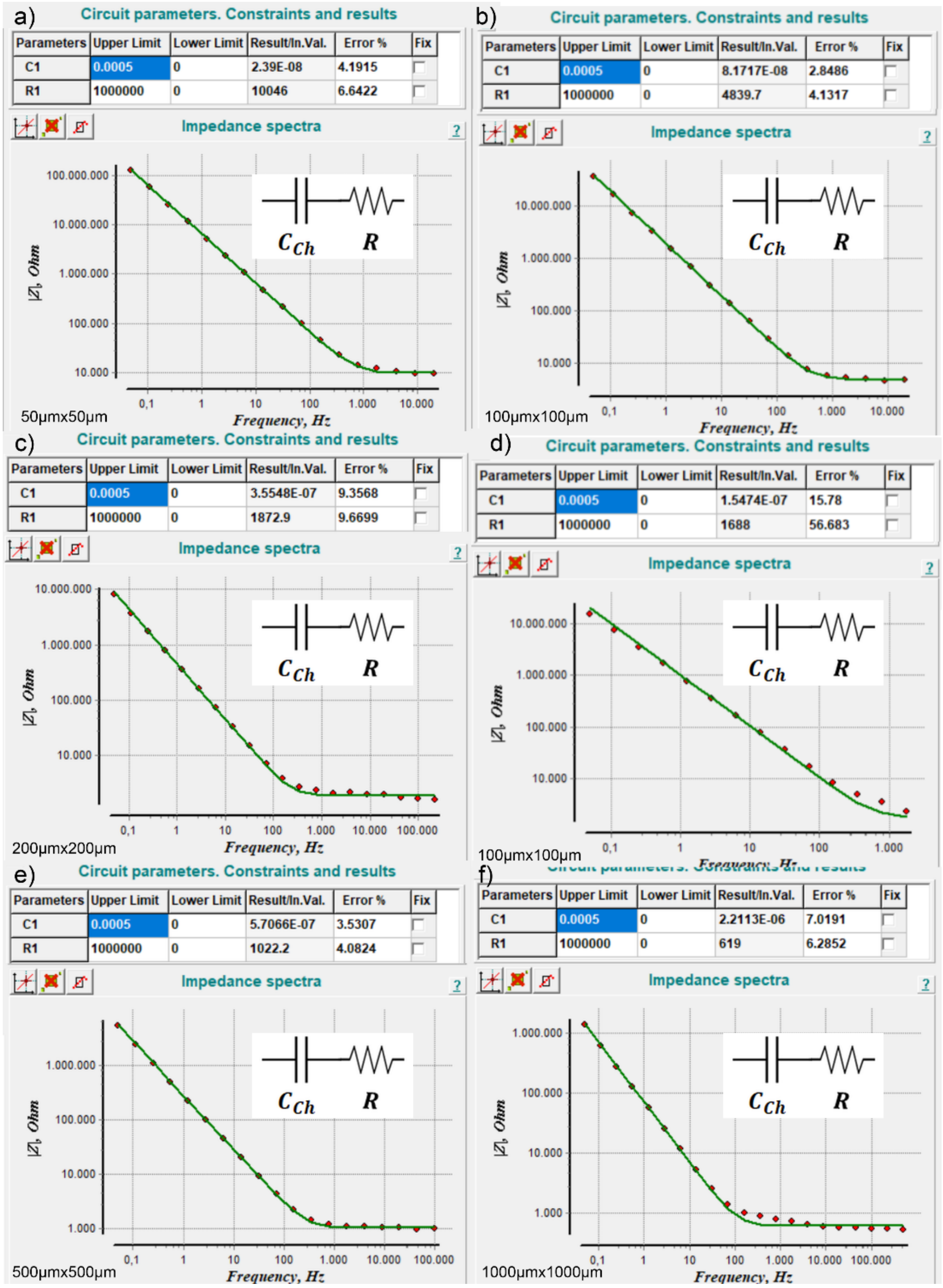

a) Circuit parameters. Constraints and results

Parameters	Upper Limit	Lower Limit	Result/In.Val.	Error %	Fix
C1	0.0005	0	2.39E-08	4.1915	☐
R1	1000000	0	10046	6.6422	☐

b) Circuit parameters. Constraints and results

Parameters	Upper Limit	Lower Limit	Result/In.Val.	Error %	Fix
C1	0.0005	0	8.1717E-08	2.8486	☐
R1	1000000	0	4839.7	4.1317	☐

c) Circuit parameters. Constraints and results

Parameters	Upper Limit	Lower Limit	Result/In.Val.	Error %	Fix
C1	0.0005	0	3.5548E-07	9.3568	☐
R1	1000000	0	1872.9	9.6699	☐

d) Circuit parameters. Constraints and results

Parameters	Upper Limit	Lower Limit	Result/In.Val.	Error %	Fix
C1	0.0005	0	1.5474E-07	15.78	☐
R1	1000000	0	1688	56.683	☐

e) Circuit parameters. Constraints and results

Parameters	Upper Limit	Lower Limit	Result/In.Val.	Error %	Fix
C1	0.0005	0	5.7066E-07	3.5307	☐
R1	1000000	0	1022.2	4.0824	☐

f) Circuit parameters. Constraints and results

Parameters	Upper Limit	Lower Limit	Result/In.Val.	Error %	Fix
C1	0.0005	0	2.2113E-06	7.0191	☐
R1	1000000	0	619	6.2852	☐

Figure S3: Fitting of the impedance data of Figure S2 to the R-C equivalent model. The wxd footprints of the vertical channel OECTs are: a) 50 µm x 50 µm b) 100 µm x 100 µm (thin PEDOT:PSS film) c) 200 µm x 200 µm d) 100 µm x 100 µm (thick PEDOT:PSS film) e) 500 µm x 500 µm and f) 1 000 µm x 1 000 µm.Table S1 presents the geometrical characteristics of the vOECTs, the spreading resistance R and the channel capacitance C_{Ch}.

	Width (W) [μm]	Thickness (d) [μm]	Capacitance C_{ch} [μF]	Spreading Resistance R [Ω]	Length (L) [nm]
vOECT 1	50	50	0.024	10 046	246
vOECT 2	100	100	0.082	4 839.7	210
vOECT 3	200	200	0.355	~~1 668~~1 872.9	227
vOECT 4	100	100	0.155	~~1 872.9~~1 688	397
vOECT 5	500	500	0.571	1 022.2	59
vOECT 6	1000	1000	2.211	619	57

Table S1: The features of the vertical channel OECTs.

Table S2 presents the calculated τ, on/off ratio and mobility values for the vertical channel OECTs. The τ values are calculated from the formula τ=R C_{Ch}. The "on-state" current is measured at V_{gs}=0 and V_{ds}=-0.6 V and the "off-state" current is measured at V_{gs}=+1V and V_{ds}=-0.6 V. The linear regime mobility values are calculated at the maximum transconductance via the formula:

$$\mu = \frac{\partial I_D}{\partial V_G} \frac{L}{W C_I V_d} \quad (S1)$$

where I_D is the channel current, V_G is the gate voltage, L is the channel length, W is the channel width and C_I is the capacitance per unit area at the interface of the channel with the electrolyte.

	Calculated τ [μs]	on/off ratio	Mobility μ [cm^2/Vs]
vOECT 1	241.104	235.949	1.42×10^{-3}
vOECT 2	396.8554	14.74771	0.58x10-3
vOECT 3	258.54	54.60661	0.23×10^{-3}
vOECT 4	664.8795	28.63955	0.87×10^{-3}
vOECT 5	583.6762	19.99294	0.025×10^{-3}
vOECT 6	1368.609	8.3005	0.007×10^{-3}

Table S2: Calculated τ, on/off ratio and mobility values for the vertical channel OECT

Figure S4: Scaling of the time constant τ with the channel volume.

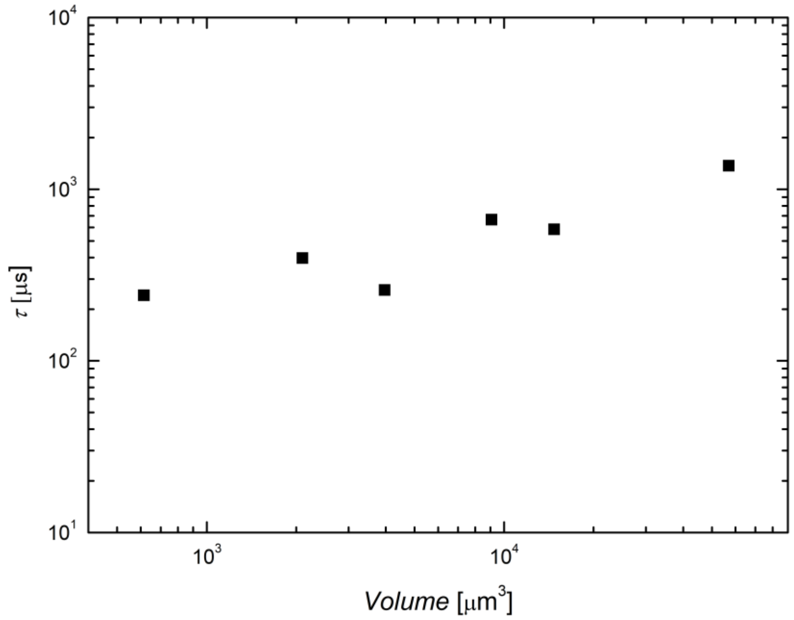

Figure S4: The increase of the channel volume results in an increase of the channel capacitance which is echoed in the increased time constant τ.

Figure S5: On/off ratio

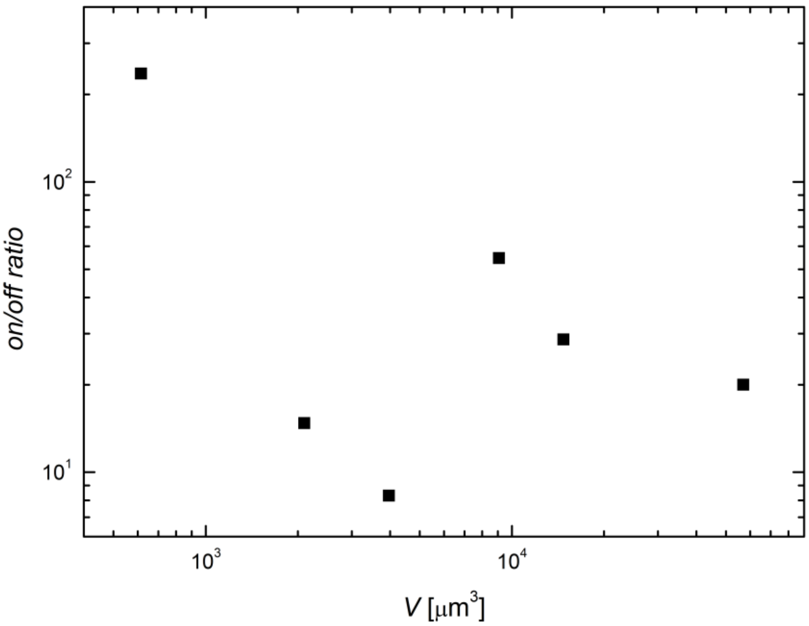

Figure S5: The on/off ratio decreases as the channel volume increases, since the PEDOT:PSS film de-dedoping process for large channel volumes becomes challenging.

Figure S6: Gate currents as a function of the gate voltage (V_{ds}=-0.6 V), for each one of the vertical OECTs presented in this work. The gate current is in the order of microamperes. For comparison, the corresponding channel current is in the order of milliamperes (Figures 2 and 3). The gate currents are measured with a dual channel Keithley 2600 SMU.

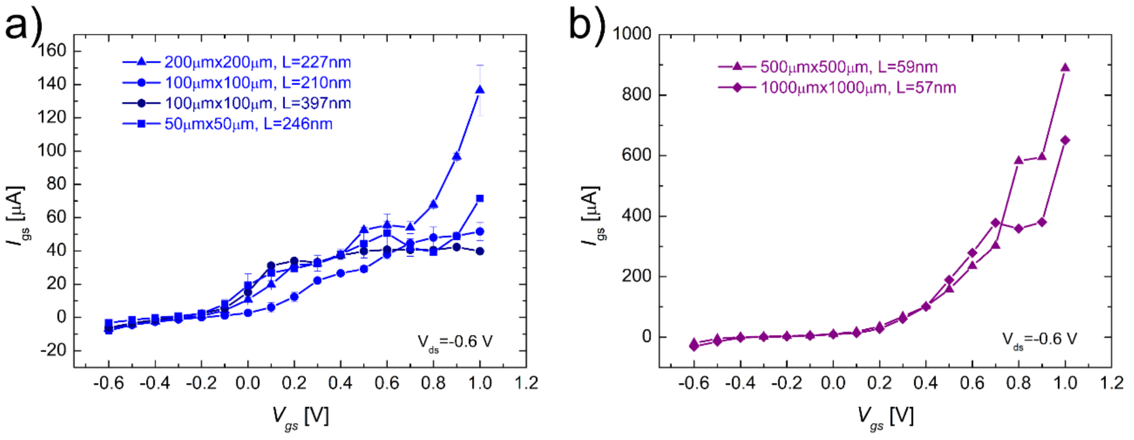

Figure S6: a) Steady state gate currents I_{gs} as a function of the gate voltage V_{gs} for the vertical OECTs with a small Wxd (50 μm x 50 μm, 100 μm x 100 μm, 200 μm x 200 μm) footprint and b) Steady state gate currents I_{gs} as a function of the gate voltage V_{gs} for the vertical OECTs with a large Wxd (500 μm x 500 μm, 1000 μm x 1000 μm) footprint.

Table S3 benchmarks the vertical channel OECT transconductance of this work with the highest ones reported in the literature.

Channel material	Electrolyte	Wd/L [μm]	g_m [mS]	Mobility μ [cm^2/Vs]	Ref.
PEDOT:PSS	0.1 M NaCl	5.4	22	1.9	1
PEDOT:PSS/[EMIM][PF6]/DBSA	PBS	6	22.7		2
p(g2T-TT)	0.1 M NaCl	2	50		3
PEDOT:PSS/Triton X-100	Poly(vinyl alcohol) hydrogel	10	54	2.4	4
PEDOT:PSS (Step-edge vertical transistor geometry)	0.1 M NaCl	28	57		5
PEDOT:PSS (Vertical channel geometry)	Ion gel	50	68.88		6
PEDOT:PSS/[EMIM][PF6]/DBSA (Interdigitated Au Electrodes)	PBS	32 000	180		2
PEDOT:PSS (Vertical channel geometry-electropolymerized channel)	0.1 M NaCl	17 543 860	498	1.42×10^{-3}	This work

Table S3: Comparison between the reported transconductance values of different state-of-the-art devices.

Table S4 compares the vertical channel OECT drain current to the gate current at V_{ds}=-0.6V and V_{gs}= 0. I_{ds} is in the mA regime while I_{gs} in the μA regime. The I_{ds}/I_{gs} current ratio is between 1 000 and 15 800.

Device	I_{ds} [A] at V_{ds}=-0.6V and V_{gs}=0	I_{gs} [A] at V_{ds}=-0.6V and V_{gs}=0	I_{ds}/I_{gs} ratio
50μmx50μm(246nm)	19.33×10^{-3}	19.30×10^{-6}	1 002
100μmx100μm(210nm)	36.04×10^{-3}	2.75×10^{-6}	13 105
200μmx200μm (227nm)	37.10×10^{-3}	10.79×10^{-6}	3 438
100μmx100μm(397nm)	27.52×10^{-3}	15.18×10^{-6}	1 813
500μmx500μm (59nm)	113.09×10^{-3}	10.30×10^{-6}	10 980
1000μmx1000μm (57nm)	149.57×10^{-3}	9.44×10^{-6}	15 844

Table S4: The table compares the drain current I_{ds} to the gate current I_{gs} at V_{ds}=-0.6V and V_{gs}= 0 for every transistor, and shows that the drain current is in the mA regime while the gate current in the μA regime. The drain current is, for every available device, from 1 000 up to 15 800 times larger than the gate current.

Table S5 presents the current densities of the vertical channel OECTs. For comparison the current density of vertical OFETs is also presented.

Device	Current density [μA/μm^{2}]	Current density [A/cm^{2}]	Ref.
50μmx50μm(246nm) PEDOT:PSS	7.732	773.2	This work
100μmx100μm(210nm) PEDOT:PSS	3.604	360.4	This work
200μmx200μm (227nm) PEDOT:PSS	0.9275	92.75	This work
100μmx100μm(397nm) PEDOT:PSS	2.752	275.2	This work
500μmx500μm (59nm) PEDOT:PSS	0.45236	45.236	This work
1000μmx1000μm (57nm) PEDOT:PSS	0.14957	14.957	This work
PDPP		1.04 M (at V_{ds}=-0.3 V)	7
P3HT		0.05-0.11 (at V_{ds}=2V)	8
C_{60} (organic permeable-base transistor (OPBT))		100 (at 2V)	9
SWCNT		80 (at V_{ds}=-1V)	10
BTQBT		1 (at V_{ds}=-3V)	11

Table S5: The current density of the vertical OECTs of this work is calculated at at V_{gs}=0 and V_{ds}=-0.6 V. The operation voltages V_{ds} of the OFETs are also presented.

Figure S7: Output curves of every reported device. The drain current values are mean values of three measurements (n=3) unless otherwise stated. The error bars denote the standard deviation of the data.

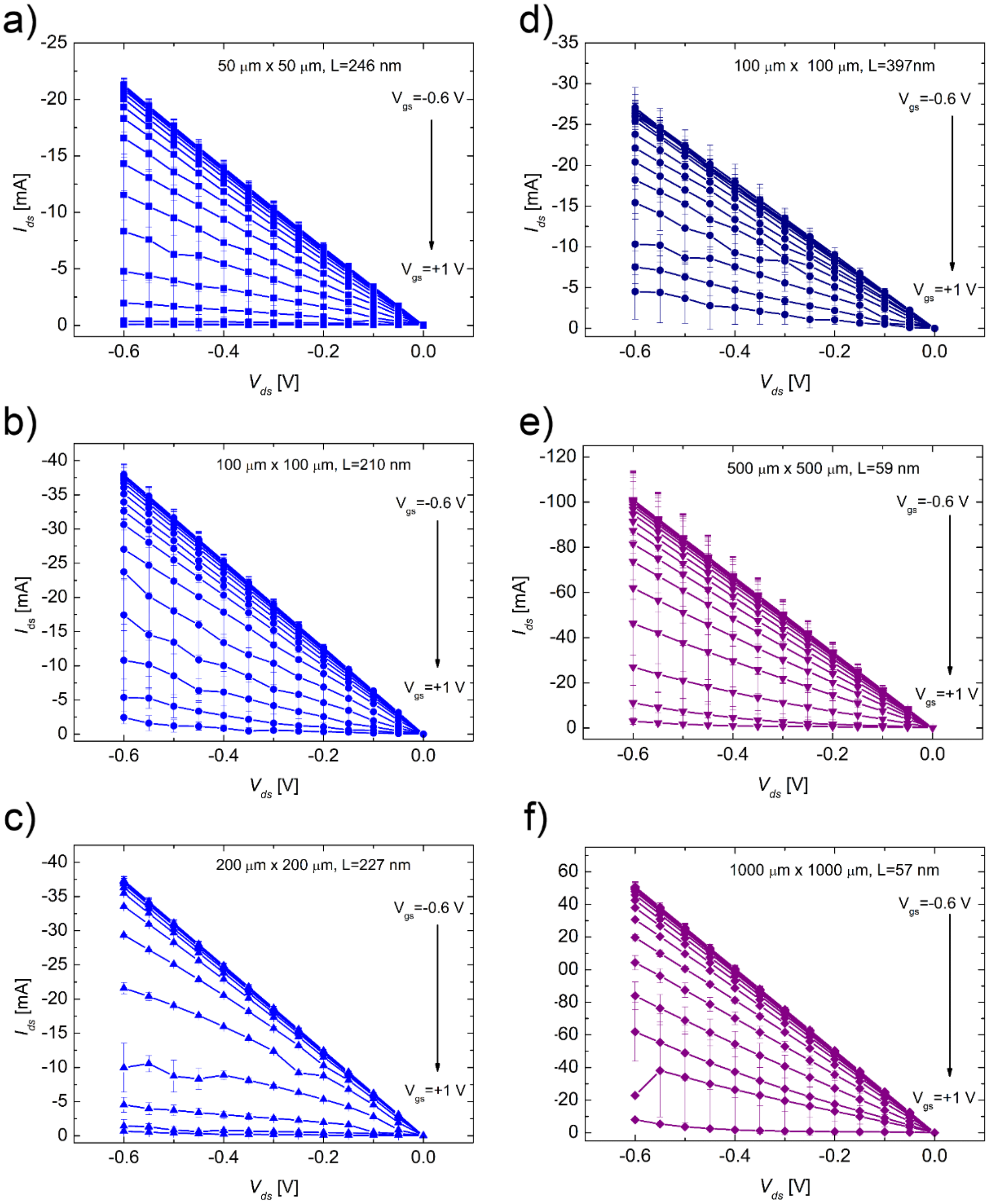

Figure S7: Output curves of every presented vertical OECT. The drain current value is the mean value of 3 measurements (n=3), unless otherwise stated. The error bars denote the standard deviation of the dataset a) 50 µm x 50 µm, L=246nm (n=2) b) 100 µm x 100 µm, L=210nm c) 200 µm x 200 µm, L=227nm d) 100 µm x 100 µm, L=397nm e) 500 µm x 500 µm, L=59nm f) 1000 µm x 1000 µm, L=57nm (n=2). For the output curves, the drain voltage sweeps from 0 to -0.6 V with a -0.05 V voltage step and the gate voltage from -0.6 V to +1 V with a +0.1 V voltage step. All measurements were carried out in 0.1 M NaCl.

References

[1] J. Rivnay, P. Leleux, M. Ferro, M. Sessolo, A. Williamson, D. A. Koutsouras, D. Khodagholy, M. Ramuz, X. Strakosas, R. M. Owens, C. Benar, J.-M. Badier, C. Bernard, G. G. Malliaras, Science Advances 2015, 1, e1400251.
[2] L. Wang, Q. Sun, L. Zhang, J. Wang, G. Ren, L. Yu, K. Wang, Y. Zhu, G. Lu, H.-D. Yu, Macromolecular Rapid Communications, n/a, 2200212.
[3] V. Venkatraman, J. T. Friedlein, A. Giovannitti, I. P. Maria, I. McCulloch, R. R. McLeod, J. Rivnay, Adv Sci (Weinh) 2018, 5, 1800453
[4] J. Ko, X. Wu, A. Surendran, B. T. Muhammad, W. L. Leong, ACS Applied Materials & Interfaces 2020, 12, 33979
[5] M. J. Donahue, A. Williamson, X. Strakosas, J. T. Friedlein, R. R. McLeod, H. Gleskova, G. G. Malliaras, Advanced Materials 2018, 30, 1705031
[6] Y. Yan, Q. Chen, X. Wang, Y. Liu, R. Yu, C. Gao, H. Chen, T. Guo, ACS Applied Materials & Interfaces 2021, 13, 7498
[7] J. Lenz, F. Del Giudice, F. R. Geisenhof, F. Winterer, R. T. Weitz, Nat Nanotechnol 2019, 14, 579.
[8] H.-W. Zan, Y.-H. Hsu, H.-F. Meng, C.-H. Huang, Y.-T. Tao, W.-W. Tsai, Applied Physics Letters 2012, 101, 093307.
[9] M. P. Klinger, A. Fischer, F. Kaschura, J. Widmer, B. Kheradmand-Boroujeni, F. Ellinger, K. Leo, Scientific Reports 2017, 7, 44713.
[10] M. Rother, A. Kruse, M. Brohmann, M. Matthiesen, S. Grieger, T. M. Higgins, J. Zaumseil, ACS Applied Nano Materials 2018, 1, 3616.
[11] H. Fukagawa, Y. Watanabe, K. Kudo, J.-i. Nishida, Y. Yamashita, H. Fujikake, S. Tokito, T. Yamamoto, AIP Advances 2016, 6, 045010